PAPER Special Section on Novel Device Architectures and System Integration Technologies

High-Frequency Low-Noise Voltage-Controlled *LC*-Tank Oscillators Using a Tunable Inductor Technique

Ching-Yuan YANG[†a)], *Member and* **Meng-Ting TSAI**[†], *Nonmember*

SUMMARY This paper describes 3-GHz and 7-GHz tunable-inductance *LC*-tank voltage-controlled oscillators (VCOs) implemented in 0.18-μm CMOS technology. Unlike the traditional tuning method by a varactor, a tunable inductor is employed in the VCO by using a transformer to compensate for the energy loss. The VCO facilitates the tuning frequency and low noise of the output signals, together with a variable inductor which satisfies both criteria. The 3-GHz VCO using a symmetry transformer provides the tuning range of 2.85 to 3.12 GHz at 1-V supply. The power consumption is 4.8 mW while the measured phase noise is −126 dBc/Hz at 1-MHz offset from a 2.85-GHz carrier. A small-area stacked transformer is employed in the 7-GHz VCO, which achieves a tuning range of 6.59 to 7.02 GHz and measured phase noise of −114 dBc/Hz at 1-MHz offset from a 6.59-GHz carrier while consuming 9 mW from a 1.2-V supply.

key words: *LC VCO, tunable inductor, high Q, transformer*

1. Introduction

LC-tank voltage-controlled oscillators (VCOs) are widely used in RF communication systems, particularly in applications of phase-locked loops (PLLs). The performance of *LC*-based oscillators heavily depends on the quality of inductors and capacitors. The mostly used approach of on-chip inductors is the spiral inductor made of metal tracks available. A spiral inductor can be made of single metal layer, which is furthest from the conductive substrate and is usually the thickest metal layer. However, the typical quality factor (Q) of on-chip spiral inductor is nearly less than eight in standard digital CMOS process. To synthesize the specified frequency band under all conditions, the VCO must provide an adequate range. Since it is difficult to vary the value of monolithic inductors in *LC* oscillators, the tank includes a voltage-dependent capacitor, i.e., varactor, to tune oscillating frequencies.

Besides the fixed inductors and the varactors, the tunable inductor techniques have been developed for RF design. The devices are divided into two types: active and passive components. Many active circuits that realize variable inductive impedance characteristics have been proposed as a solution to replace the passive inductor [1], [2]. The inductance realized by these circuits is proportional to a capacitance and inversely proportion to the square of a transconductance, necessitating relatively high-bias currents to achieve a RF inductance value, and thereby results in significant power consumption and noise. Considering passive inductive components, on the contrary, transformer-based Q-enhancement techniques have demonstrated good performance at radio frequencies [3], [24]. In this paper, a tunable coupled inductance technology using monolithic spiral transformer is developed for a high-frequency low-noise *LC*-VCO design. The proposed oscillator does not employ a varactor but a tunable inductor for frequency control. To address this issue, we consider underlying physics of a two-port transformer, concluding that the selection of tunable inductance and high Q plays a central role. An investigation of these properties leads to a design strategy based on an *LC*-VCO scheme, providing high-frequency and low-noise performance. In this work, two VCOs with different structure of transformers were implemented in a 0.18-μm CMOS process for 3-GHz and 7-GHz operations, respectively.

The paper is organized as follow. Section 2 presents the basic concept of the tunable inductor by using a two-port transformer. Section 3 and Sect. 4 describe the proposed *LC*-VCO circuit realization, the chip implementation and the measurement of the circuits, respectively, and Sect. 5 gives the conclusion at last.

2. Tunable Inductor by Using a Two-Port Transformer

2.1 Basic Concept and Analysis

Here, we will introduce a two-port transformer as a circuit element and perform a simplified analysis to obtain essential understanding of the basic tunable inductor. In analyzing a circuit containing a transformer, it is common practice to eliminate the transformer by reflecting impedances from one side of the transformer to the other. As shown in Fig. 1, a simplified two-port transformer consists of a primary coil (v_1, i_1) at port 1 and a secondary coil (v_2, i_2) at port 2 with self-inductances L_1 and L_2, respectively. R_1 and R_2 are included to account for the losses in the coils. They are the series parasitic resistances associated with the primary and the secondary coils. The inductive coupling coefficient be-

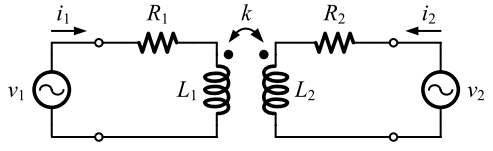

Fig. 1 Simplified two-port transformer.

Manuscript received April 10, 2006.
Manuscript revised June 19, 2006.

[†]The authors are with the Department of Electrical Engineering, National Chung Hsing University, Taichung, Taiwan, R.O.C.
a) E-mail: ycy@dragon.nchu.edu.tw

DOI: 10.1093/ietele/e89–c.11.1567

tween the two coils is modeled by k. The coupling coefficient is a measure of the magnetic coupling between two coils; $0 \le k \le 1$. Note that the parasitical capacitances and the substrate loss are ignored for ideally high self-resonant frequencies. The object is to use the secondary coil as a conduit to compensate for the energy loss in the primary coil [4]. If two source generators have the same frequency and are applied to the two ports, then two equations can be formulated for the voltage between port 1 and port 2 in matrix form and we get

$$\begin{bmatrix} v_1 \\ v_2 \end{bmatrix} = \begin{bmatrix} R_1 + j\omega L_1 & j\omega M \\ j\omega M & R_2 + j\omega L_2 \end{bmatrix} \begin{bmatrix} i_1 \\ i_2 \end{bmatrix} \tag{1}$$

where M is the mutual inductance which is related to k by

$$M = k\sqrt{L_1 L_2} \tag{2}$$

If the source in port 2 is sampled from the port 1, then their relation can be represented by

$$v_2 = v_1 A\angle\theta \tag{3}$$

where A is transfer gain and θ is the phase difference between v_1 and v_2. By solving Eqs. (1) and (3), the input impedance to port 1 is

$$Z_{in} = \frac{v_1}{i_1} = \frac{(R_1 + j\omega L_1)(R_2 + j\omega L_2) + \omega^2 M^2}{(R_2 + j\omega L_2) - j\omega MA\angle\theta} \tag{4}$$

Equation (4) can be also written as $R_{eq}(\omega) + j\omega L_{eq}(\omega)$, where R_{eq} and L_{eq} are the equivalent resistance and inductance, respectively. Then, we have

$$R_{eq}(\omega) = \frac{WX + \omega^2 YZ}{X^2 + \omega^2 Z^2} \tag{5}$$

$$L_{eq}(\omega) = \frac{XY - WZ}{X^2 + \omega^2 Z^2} \tag{6}$$

where $W = R_1R_2 - \omega^2 L_1 L_2 + \omega^2 M^2$, $X = R_2 + \omega AM \sin\theta$, $Y = R_1L_2 + R_2L_1$, and $Z = L_2 - AM\cos\theta$. To verify the value of the input impedance at port 1 to gain A, the element set $\{L_1, R_1, L_2, R_2, k\}$ of the transformer is given to {3.12 nH, 2.54 Ω, 3.12 nH, 2.54 Ω, 0.6} as an example to explain. Figure 2 shows how resistive part R_{eq} and inductive part L_{eq} at 3 GHz vary for different values of A and θ. Considering both tuning range and feasibility of the practical circuitry, in this design the value of θ is taken into zero for getting larger tuning range of inductance as A varies. As observed, the inductance increases as gain does, and thereby we will use this characteristic to make a variable inductor. To view the performance of the primary coil when $\theta = 0$, the quality factor Q defined as the ratio of the imaginary part to the real part, i.e., $Q = \omega L_{eq}/R_{eq}$, is shown in Fig. 3. It can be found that Q is increased when the gain increases. As approaching high-gain region, moreover, the resistance decreases while the reactance increases.

Although Fig. 3 provides essential insights into the oscillation noise as a function of gain, how to implement an electrical oscillator is a more practical design work. Two important concepts of low noise performance and tuning range

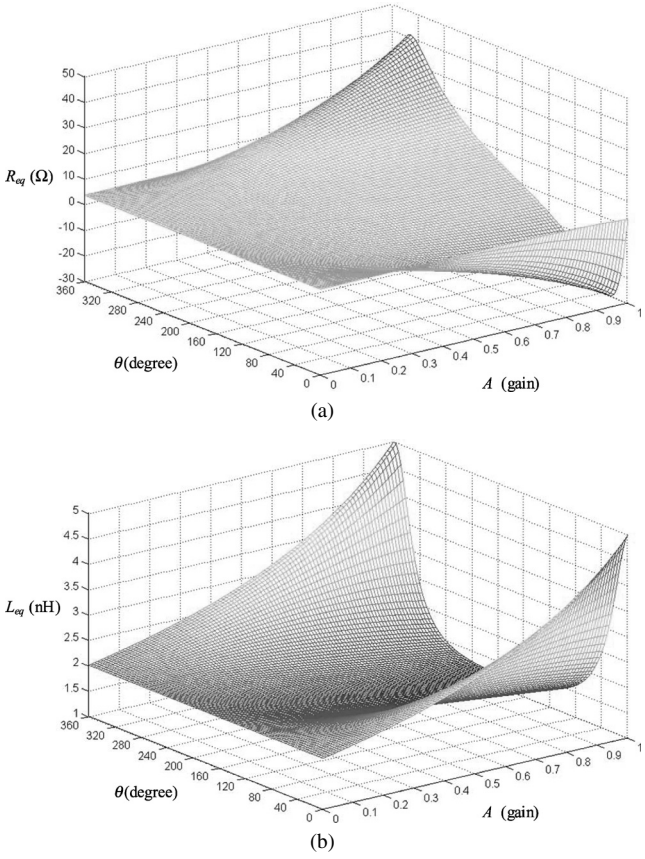

Fig. 2 Input impedance characteristics to the port 1 of the transformer at $f = 3$ GHz: (a) the equivalent resistance, and (b) the equivalent inductance.

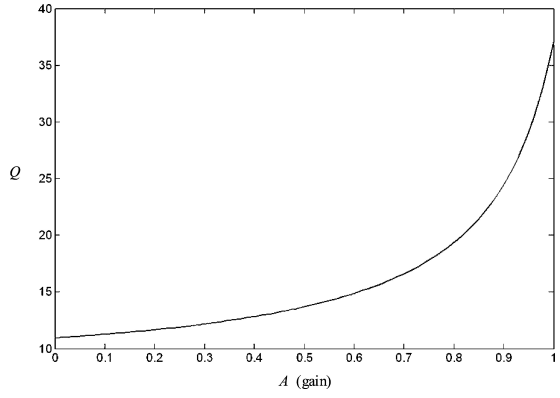

Fig. 3 Quality factor of the port 1 as $\theta = 0$.

in the design regime have to be considered. It can be viewed that the Q of the transformer-based inductor is larger than 10 in Fig. 3. Thus the employed coupling can improve the characteristics of the inductor. To obtain better performance for the LC oscillators in advance, the gain is designed to larger than 0.7 in our design.

2.2 Transformer Realization

A monolithic transformer can be realized either by tapping into a series of turns of coupled micro-strip lines or by inter-

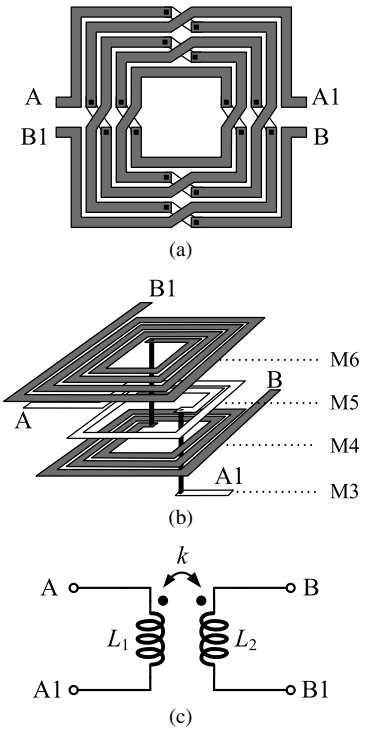

Fig. 4 Transformers: (a) symmetry topology, (b) sandwich-stacked topology, and (c) symbol.

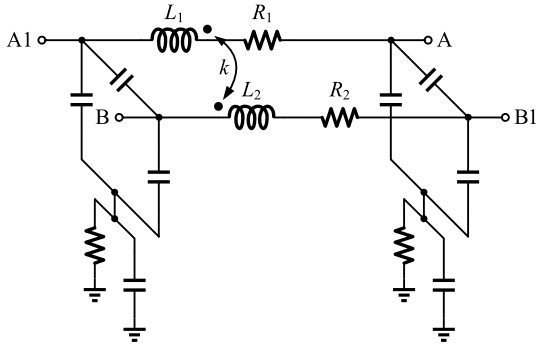

Fig. 5 A lumped-element circuit model for the transformers.

winding two spiral inductors. The tapped structure can provide an arbitrary turn ratio, but it is not perfectly symmetrical for 1:1 turns ration case [5], [6]. Figure 4(a) shows the structure of a two-port symmetric transformer, suited for differential applications. It has been recognized that the quality factor of an inductor at high frequency is higher seen differentially than single-endedly [7]. In some cases, circuits requiring large inductance values can incorporate stacked structures to save substantial area. Depicted in Fig. 4(b) is a metal sandwich transformer, where two stacked spirals are placed in series, yielding a large inductance in the secondary. However, the primary and secondary coils are not symmetry, thereby will result in effects in a differential VCO. Figure 5 shows the the lumped-element circuit model of the transformers, which can be partitioned into a pair of coupled spiral inductors including capacitive effect and substrate loss [8], [9].

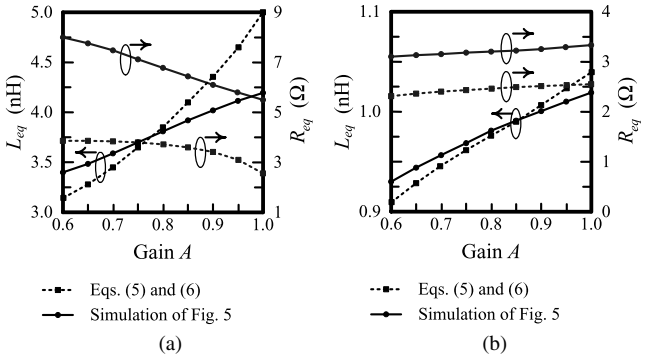

Fig. 6 Simulated characteristics of the tunable transformer-based inductors as gain is a variable: (a) symmetry topology for 3-GHz operation, and (b) sandwich-stacked topology for 7-GHz operation.

The above two types of transformers, the symmetric one (T1) and the stacked one (T2), will be employed in our VCOs to verify their performance. T1 is made of the top metal layer, i.e., metal 6 layer, and T2 consists of metal 5 layer to form the primary coil and metal 6 and metal 4 layers to form the secondary one. In T1 L_1 is equal to L_2 because of symmetric characteristic, whereas L_1 is smaller than L_2 in T2. The main element sets $\{L_1, R_1, L_2, R_2, k\}$ of T1 and T2 are given to {3.12 nH, 2.54 Ω, 3.12 nH, 2.54 Ω, 0.6} and {1.75 nH, 0.9 Ω, 14.31 nH, 18.7 Ω, 0.75}. Also, their operating frequencies are associated to 3 GHz and 7 GHz, respectively. Figure 6 shows their simulated characteristics of equivalent inductances and equivalent resistances for the monolithic transformers by the model of Fig. 5 and the simplified ones described by Eqs. (5) and (6) as $\theta = 0$, ignoring substrate loss and parasitic capacitors. In comparison, the resistances of monolithic transformers get larger due to substrate loss and result in reducing Q. As observed, the tuning range of inductances is decreased and will affect the frequency range of VCOs. The overall simulated Q is more than 8, and it rises as the gain increases.

3. VCO Circuit Implementation

3.1 Basic *LC* Oscillator

A general push-pull *LC*-oscillator circuit scheme is shown in Fig. 7 [10], [11]. The double cross-connection of an NMOS (M_{n1}-M_{n2}) and a PMOS (M_{p1}-M_{p2}) differential pairs in positive feedback generates an negative resistance to compensate the parasitic parallel resistance of *LC* tank for oscillation to occur. The capacitance of the tank can be formed from an effective parasitic capacitor (C_p) and a varactor. The frequency-tuning varactor, as shown in the dotted circle, is represented as a voltage-controlled variable capacitor (C_v) in shunt with a non-variable capacitor (C_0). Thus, the resonant capacitances of the *LC* tank can be simplified to be regarded as the sum of constant capacitances and tunable ones. The former are mainly made of the parasitic capacitances of the inductor, the varactor and the transistors, and further limit

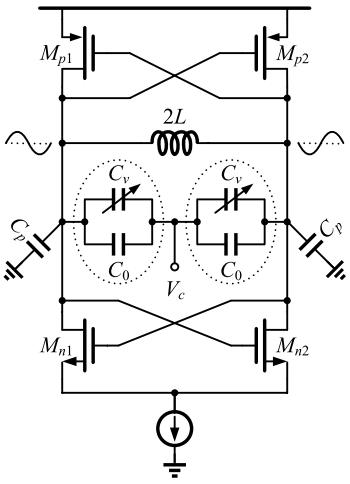

Fig. 7 One traditional *LC*-VCO.

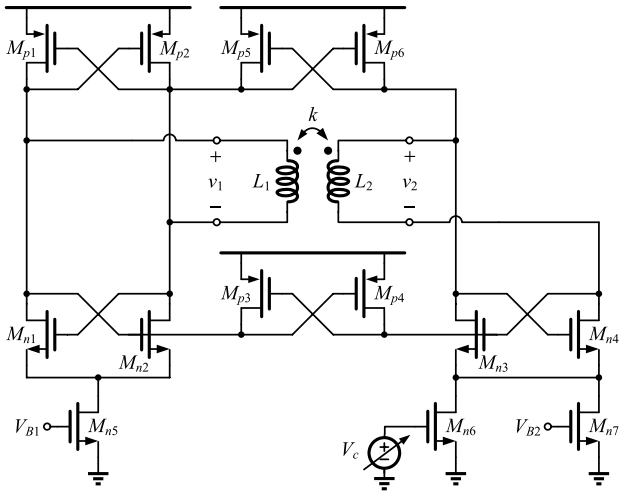

Fig. 8 The proposed *LC*-VCO with a transformer-based tunable inductor.

the tuning range even reduce the operating frequencies because they cannot be varied by the control voltage. In order to maximize both the tuning range and the operating frequencies, constant capacitances in the tank must be minimized. It nevertheless suffers from a trade-off between the dynamic range and the operating frequency. This is because, for using a given inductance in higher frequency operation, the parasitic capacitances from the transistors constitute a significant fraction of the overall capacitance, thereby limiting the tuning range.

Besides, the varactor capacitance spans a portion of its *C*-*V* curve that depends on the control voltage (V_c) and the bias as well as the signal amplitude. Since the actual voltage applied across to non-linear characteristic varactor device terminals is composed of DC voltage and large signal AC voltage, the *C*-*V* curve calculated for DC voltage differs from the large signal AC voltage [12]. Therefore, the *C*-*V* curve under large signal condition depends on the amplitude of the signal applied across its terminals along with DC voltage. The effective capacitance is obtained through averaging the instantaneous capacitance over one oscillation period for VCO operation.

3.2 Proposed *LC*-VCO Using a Tunable Transformer-Based Inductor

To replace the varactor, the *LC*-based oscillator scheme with a tunable transformer-based inductor is shown in Fig. 8. The VCO circuit is divided into two parts: one is the *LC* oscillation scheme and the other is the tuning one. The *LC* oscillation scheme formed by M_{n1}-M_{n2} and M_{p1}-M_{p2} is the same that in Fig. 7 but without the varactor in the primary coil of the transformer, while the tuning circuit appears in the secondary. The resonant circuit is generally the type of parallel *LC*-tank, which is formed by the equivalent inductance from the primary coil of the transformer and the parasitic capacitances across the port. Here, M_{p3}-M_{p4} and M_{p5}-M_{p6} can act as high-speed latches in positive feedback phase. Their terminals has voltage complements, so that their output voltages are merely opposite phases. M_{p3} and M_{p5} couple the signal from the v_2; on the contrary the tuning circuit samples v_1 by M_{p4} and M_{p6}. M_{p4} and M_{p6} convert v_1 to a differential current and inject the result into the secondary coil. The cross-connection of the M_{n3}-M_{n4} differential pair in positive feedback forms a negative resistance to suppress the resistive effect in the secondary coil but not to make oscillation. M_{n5}, M_{n6} and M_{n7} provide DC trail current for biasing the circuit of the primary and secondary sides. V_c is the control voltage to vary the gain of A between v_1 and v_2, thereby changes the inductance and its Q of the primary in the tank. Note that although the control voltage is approach to zero, even all transistors of the tuning scheme turn off, the gain is not zero because of the coupling effect of the transformer.

If the negative resistance provided by the cross-coupled pair exactly cancels the loss of the secondary coil of the transformer, it will be at the edge of oscillation in the tuning block. In this way two oscillating blocks may appear in the terminals of the two-port transformer and their signals couple each other. If their oscillation frequencies are the same, it will result in in-phase coupling and force their output to remain in phase [13]; if not, the oscillation signals are coupling together and get a complicated phenomenon. We must keep the tuning circuit from oscillating; thereby the transconductance of M_{n3}-M_{n4} should be lower by a well controlled bias.

3.3 Simplified Linear Analysis

To understand the operation, we exploit the coupling model of Fig. 9(a) to construct the equivalent circuit shown in Fig. 8. R_1-R_2 and C_{p1}-C_{p2} represent the parasitic resistances and capacitances. Note that $G_{m1} = g_{mp3,5}$, $G_{m2} = g_{mp4,6}$, $-R_a = -1/(g_{mn1,2} + g_{mp1,2})$, and $-R_b = -1/(g_{mn3,4})$. To simplify Fig. 9(a), the simple equivalent circuit is shown in Fig. 9(b). From simulation in the next section, their phase difference is very small, so that $v_2 \approx Av_1$. Besides, nonlinear active circuit is used to implement the negative resis-

tance [14]. At the edge of oscillation, $-R$ exactly cancels the loss in the primary. As discussed in Sect. 2.1, the effective inductance of Eq. (6) in the primary becomes

$$L_{eff} \approx \frac{\omega^2(L_2 - AM)(L_1L_2 - M^2)}{\omega^2(L_2 - AM)^2 + R_2^2} + \frac{R_2(R_2L_1 - AR_1M)}{\omega^2(L_2 - AM)^2 + R_2^2} \tag{7}$$

At resonance, $\omega_0^2 = 1/L_{eff}C_{p1}$, where ω_0 is oscillation frequency. Then we have

$$\omega_0^2 = \frac{-B + \sqrt{B^2 - 4AC}}{2A} \tag{8}$$

where $A = C_{p1}(L_2 - AM)(L_1L_2 - M^2)$, $B = R_2C_{p1}(R_2L_1 - AR_1M) - (L_2 - AM)^2$, and $C = -R_2^2$. Suggesting only the inductor and capacitor values can vary to tune the frequency and other parameter such as resistances affect f_{osc} negligibly, i.e., $R_1 \approx 0$ and $R_2 \approx 0$, we get

$$\omega_0^2 = \frac{L_2 - AM}{(L_1L_2 - M^2)C_{p1}} \tag{9}$$

In fact, the oscillation frequency is determined by the effective inductance and effective capacitance in the primary terminals, which include the reflecting effects from the secondary part [15]. It can be seen that the effective capacitance is somewhat more than C_{p1} and lowers the operating frequency. Considering high-frequency operation, therefore, the parasitic capacitances in both primary and secondary parts should be reduced. The circuit of Fig. 9(a) can be transformed to an equivalent topology of Fig. 9(c) that more easily leads to analysis, where R_{p1} and R_{p2} represent the equivalent parallel resistances. The voltage in the secondary coil can be given by

$$v_2 = R_{p2}\left(G_{m2}v_1 - i_2 - j\omega C_2 v_2\right) \tag{10}$$

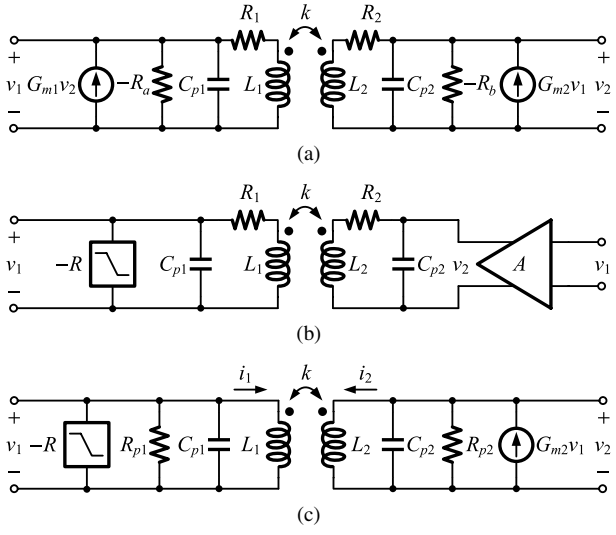

Fig. 9 (a) Small-signal equivalent circuit of Fig. 8, (b) simplified equivalent circuit, and (c) equivalent circuit with equivalent parallel resistors.

It follows that

$$\frac{v_2}{v_1} = \frac{\omega G_{m2}R_{p2}\left(L_1L_2 - M^2\right) - jR_{p2}M}{\omega\left(L_1L_2 - M^2\right) + jR_{p2}\left[\omega^2 C_{p2}\left(L_1L_2 - M^2\right) - L_1\right]} \tag{11}$$

To arrive at tuning technique, Eq. (11) exhibits G_{m2} and R_{p2} that can be controlled by the bias current. Here, R_{p2} consists of the equivalent parallel resistance of the secondary coil, R_{Lp2}, and a negative resistance of $-1/g_{mn3,4}$ from the cross coupled pair M_{n3}-M_{n4}. As the bias current increases, the value of G_{m2} as well as the equivalent resistance $R_{p2} = R_{Lp2}\|(-1/g_{mn3,4}) = R_{Lp2}/(1 - g_{mn3,4}R_{Lp2})$ increases, thereby increases the gain. The minimum gain can be given due to the mutual coupling between the primary and secondary when G_{m2} and $g_{mn3,4}$ go to zero.

4. Simulation and Measurement Results

To verify the performance of the VCOs as previously described, the proposed circuits were fabricated in 0.18-μm CMOS technology. Two VCOs (called VCO1 and VCO2), employing the transformers of Figs. 4(a) and 4(b) respectively, are implemented in this work. Table 1 shows dimensions and features for the various components of VCOs. The transformer model of Fig. 5 is adopted. The simulated characteristics of the gain (A) and phase difference (θ) in VCO1 are shown in Fig. 10. θ is smaller than 2.2° and A is between 0.77 and 0.96. It shows the function of the tunable inductance has near in-phase between v_2 and v_1 and the gain is smaller than 1. Note that the tuning range depends on the range of the gain, controlled by the bias current.

Figure 11 shows the microphotograph of the test chip. The core circuit occupies an active area of $1.4 \times 1.4\,\text{mm}^2$ including the output buffers and I/O pads. Each output signal is connected to an open-drain circuit with an externally match resistance of 50 Ω. The VCOs were tested on an FR-4 PC board using Agilent E4407B Spectrum Analyzer for measurement. Table 2 summarizes the overall specifications of the VCOs. The minimum operating

Table 1 Dimensions and values for the VCO components.

Transistors ($W \times L$)	in μm	Transformers
M_{p1}, M_{p2}	75×0.18	T1:
M_{p3}, M_{p4}, M_{p5}, M_{p6}	75×0.18	$L_1 \approx 3.12$ nH
M_{n1}, M_{n2}	150×0.18	$L_2 \approx 3.12$ nH
M_{n3}, M_{n4}	75×0.18	T2:
M_{n5}	300×0.18	$L_1 \approx 1.75$ nH
M_{n6}, M_{n7}	150×0.18	$L_2 \approx 14.31$ nH

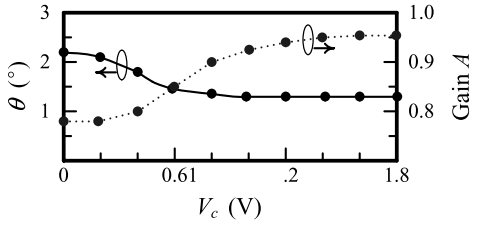

Fig. 10 Simulated characteristics of the gain and phase difference.

Table 2 VCO performance summary.

	VCO1		VCO2	
Supply voltage (V)	1		1.2	
Tuning range (GHz)	2.85–3.12		6.59–7.02	
Measured frequency (GHz)	2.85	3.12	6.59	7.02
Phase noise (dBc/Hz) @ 100 kHz	−106	−98	−103	−88
Phase noise (dBc/Hz) @ 1 MHz	−126	−118	−114	−104
Phase noise (dBc/Hz) @ 10 MHz	−146	−139	−128	−124
Dissipation current (mA)	4.8	3.4	7.5	5.3
FoM (dBc/Hz) @ 1-MHz offset frequency	−188.3	−182.6	−180.8	−172.9

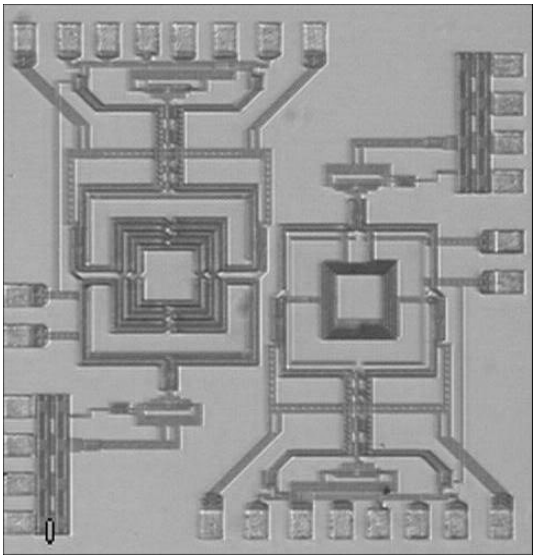

Fig. 11 Die photo of the fabricated chip consisting of two VCOs.

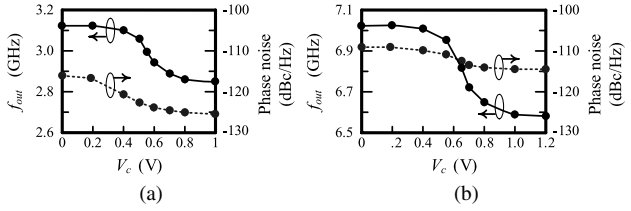

Fig. 12 Measured characteristics of tuning frequency range and phase noise value at 1-MHz offset for (a) VCO1 and (b) VCO2.

supply voltages of VCO1 and VCO2 are 1 V and 1.2 V, and they consume the maximum currents of 4.8 mA and 7.5 mA, respectively. The measured output powers of VCO1 and VCO2 are around −9 dBm and −15 dBm, respectively. The measured frequency-tuning characteristics of VCO1 are shown in Fig. 12(a). As can be seen, the tuning range is 9% (2.85 to 3.12 GHz). Figure 12(a) also shows a plot of the measured phase noise at 1-MHz offset from the carrier for the control voltages from 0 to 1.0 V. The phase noise is from −118 to −126 dBc/Hz. Similarly, the measured characteristics of VCO2 are shown in Fig. 12(b), with the tuning range of 6.3% (6.59 to 7.02 GHz) and phase noise of −104 to −114 dBc/Hz at 1-MHz offset from the carrier. As discussed in Sect. 2.1, increasing the control voltage increases the equivalent inductances but decreases the operating frequencies. Furthermore, the phase noise decreases because of increasing the Q of the resonant inductor. The minimum phase noise of the VCOs occurs at minimum operating frequencies. Figure 13 shows the phase noise of VCO1 at 2.85 GHz and VCO2 at 6.59 GHz, respectively. The measured phase noise of 2.85-GHz oscillator is −106 dBc/Hz at 100-kHz offset, −126 dBc/Hz at 1-MHz offset, and −146 dBc/Hz at 10-MHz offset, and that of 6.59-GHz oscillator is −103 dBc/Hz at 100-kHz offset, −114 dBc/Hz at 1-MHz offset, and −128 dBc/Hz at 10-MHz offset. Using a linear theory [16], an oscillator's phase-noise model is given by

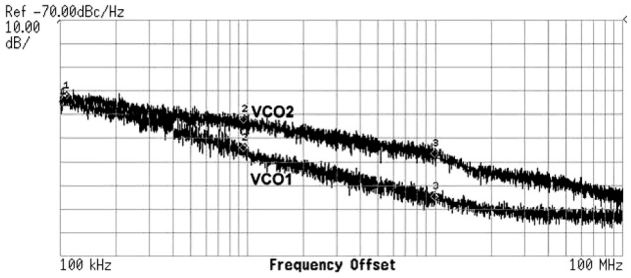

Fig. 13 Measured phase noise of VCO1 at 2.85 GHz and VCO2 at 6.59 GHz, respectively.

$$L(\Delta\omega) = 10\log\left[\frac{2FkT}{P_{\text{sig}}}\left(1+\frac{\omega_o}{2Q_{\text{tank}}\Delta\omega}\right)^2\right] \quad (12)$$

where ω_o is the center frequency, $\Delta\omega$ is the frequency offset, Q_{tank} is the tank quality factor, F is the excess noise factor, P_{sig} is the oscillation signal power, and $L(\Delta\omega)$ is the phase noise measured at $\Delta\omega$. The phase noise performance is mainly due to the characteristics of the inductor. Because of the asymmetric structure and substrate loss† of the transformer as well as higher-frequency operation, the measured phase noise of VCO2 is approximately 12 dBc/Hz worse than that of VCO1 at the same control voltage. The measured spectrum of 3 GHz and 7 GHz are shown in Fig. 14, and they prove that the resonant oscillation of the *LC*-tanks merely occurs in the primary of the transformers.

A widely accepted figure of merit (*FoM*) for VCOs is given by [17]:

$$FoM = L(\Delta\omega) - 20\log\left(\frac{\omega_o}{\Delta\omega}\right) + 10\log\left(\frac{P_{\text{diss}}}{1\,\text{mW}}\right) \quad (13)$$

†The loss mechanism arises from the magnetic coupling and the capacitance between the inductor (transformer) and the substrate [13]. This phenomenon of T2 lowers the Q due to its bottom layer more near the substrate than that of T1.

This *FoM* normalizes the phase noise at a given offset ($\Delta\omega$), the center frequency (ω_o), and the power consumption (P_{diss}) in milliwatts. The best *FoM*s of VCO1 and VCO2 are −188.3 dBc/Hz and −180.8 dBc/Hz, respectively. Table 3 shows the *FoM*s of several comparable over the past years [18]–[25]. Note that all of them use varactors for frequency tuning.

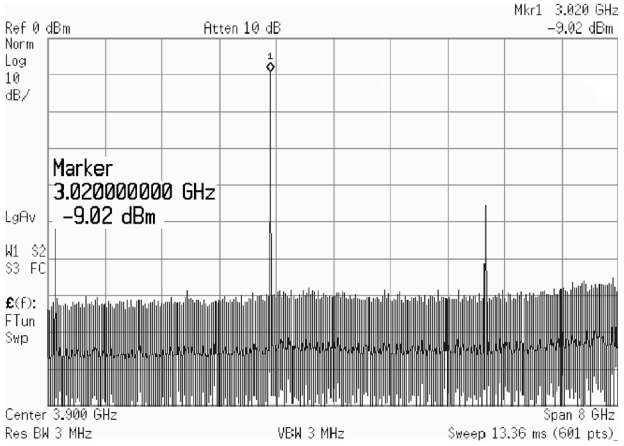

(a)

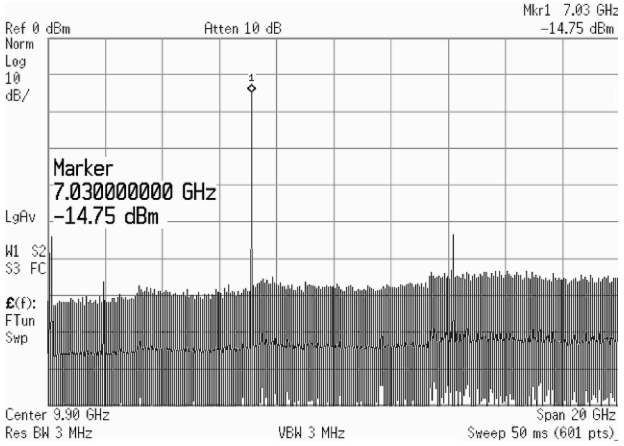

(b)

Fig. 14 Measured output power spectrum of (a) VCO1 at 3 GHz, and (b) VCO2 at 7 GHz.

5. Conclusion

It is an interesting work covering the use of tunable inductors in place of tunable capacitors e.g., varactors, for building high-frequency VCOs. In this paper, an *LC*-VCO using a tunable transformer-based inductor is proposed as the architecture choice for high-frequency low-noise applications. Two prototype *LC*-VCOs utilize the tunable inductors to extend the operating frequencies at 2.85–3.12 GHz and 6.59–7.02 GHz, respectively, in a standard 0.18-μm CMOS process at minimum operating supply voltages of 1 V and 1.2 V. The measured results demonstrate the functionality of the *LC* VCOs with the proposed tunable inductor technique.

Acknowledgments

The authors would like to thank the National Chip Implementation Center, Taiwan, for the fabrication of the chip. This work was supported by the National Science Council (NSC), Taiwan, under Contract NSC94-2220-E-005-003.

References

[1] J.-S. Ko and W. Lee, "Low power, tunable active inductor and its applications to monolithic VCO and BPF," IEEE MTT-S Int. Microw. Symp. Dig., pp.929–932, June 1997.

[2] M. Grozing, A. Pascht, and M. Berroth, "A 2.5 V CMOS differential active inductor with tunable *L* and *Q* for frequencies up to 5 GHz," IEEE MTT-S Int. Microw. Symp. Dig., pp.575–578, June 2001.

[3] B. Georgesu, H. Pekau, J. Haslett, and J. McRory, "Tunable coupled inductor *Q*-enchement for parallel resonant *LC* tanks," IEEE Trans. Circuits Syst. II, Analog Digit. Signal Process., vol.50, no.10, pp.705–713, Oct. 2003.

[4] T. Teung, Analysis and Design of On-chip Spiral Inductors and Transformers for Silicon RF Integrated Circuits, Master thesis, Hong Kong University of Science and Technology, 1998.

[5] A. Boulouard and M.L. Rouzic, "Analysis of rectangular spiral transformers for MMIC application," IEEE Trans. Microw. Theory Tech., vol.37, no.8, pp.1257–1260, Aug. 1989.

[6] L. Selmi and B. Ricco, "Design of an X-band transformer-coupled amplifier with improved stability and layout," IEEE J. Solid-State Circuits, vol.28, no.6, pp.701–703, June 1993.

[7] J.J. Zhou and D.J. Allstot, "Monolithic transformers and their application in a differential CMOS RF low-noise amplifier," IEEE J. Solid-State Circuits, vol.33, no.12, pp.2020–2027, Dec. 1998.

[8] Taiwan Semiconductor Manufacturing Co., LTD, TSMC 0.18-μm Mixed Signal 1P6M Salicde 1.8 V/3.3 V RF Spice Models, Ver.1.3, 2004.

Table 3 Comparison of performance with prior works.

Ref.	Technology [μm]	Frequency [GHz]	Power [mW]	Phase noise [dBc/Hz]	*FoM* [dBc/Hz]
[22]	0.18 CMOS	1.1	5.4	−120 @ 1 MHz	−173.5
[19]	0.35 BiCMOS	4.4	36.5	−113 @ 600 kHz	−174.7
[20]	0.25 CMOS	4	7.5	−117 @ 1 MHz	−180.3
[18]	0.65 BiCMOS	2	34.2	−126 @ 600 kHz	−181.1
[21]	0.13 SOI CMOS	5.6	2	−114 @ 1 MHz	−186.0
[23]	0.18 CMOS	1.8	2.6	−126 @ 1 MHz	−187.0
[25]	0.35 CMOS	2.9	16	−142 @ 3 MHz	−189.5
[24]	0.18 CMOS	3.8	0.57	−119 @ 1 MHz	−193.0
This work (VCO1)	0.18 CMOS	2.85/3.12	4.8/3.4	−126/−118 @ 1 MHz	−188.3/−182.6
This work (VCO2)	0.18 CMOS	6.59/7.02	9.0/6.36	−114/−104 @ 1 MHz	−180.8/−172.9

[9] J.R. Long, "Monolithic transformers for silicon RF IC design," IEEE J. Solid-State Circuits, vol.35, no.9, pp.1368–1382, Sept. 2000.
[10] K. Andreani and H. Sjoland, "Tail current noise suppression in RF CMOS VCOs," IEEE J. Solid-State Circuits, vol.37, no.3, pp.342–348, March 2002.
[11] J. Cranickx, M. Steyart, and H. Miyakawa, "A fully integrated spiral-*LC* CMOS VCO set with prescaler for GSM and DCS-1800," Proc. IEEE Custom Integrated Circuits Conf. (CICC), pp.403–406, May 1997.
[12] A. Aktas and M. Ismail, CMOS PLLs and VCOs for 4G Wireless, Kluwer Academic Publishers, 2004.
[13] B. Razavi, Design of Integrated Circuits for Optical Communications, Chapter 7, McGraw-Hill, 2003.
[14] E. Hegazi, J. Rael, and A. Abidi, The Designer's Guide to High-Purity Oscillator, Kluwer Academic Publishers, 2005.
[15] C.P. Yue and S.S. Wong, "On-chip spiral inductors with patterned ground shields for Si-based RF IC's," IEEE J. Solid-State Circuits, vol.33, no.5, pp.734–752, May 1998.
[16] D.B. Leeson, "A simple model of feedback oscillator noise spectrum," Proc. IEEE, vol.54, no.2, pp.329–330, Feb. 1966.
[17] P. Kinget, Integrated GHz Voltage Controlled Oscillators, Kluwer Academic Publishers, New York, 1999.
[18] B. Muer, M. Borremans, M. Steyaert, and G. Puma, "A 2-GHz low-phase-noise integrated *LC*-VCO set with flicker-noise upconversion minimization," IEEE J. Solid-State Circuits, vol.35, no.7, pp.1034–1038, July 2000.
[19] P. Vaananen, M. Metsanvirta, and N.T. Tchamov, "A 4.3-GHz VCO with 2-GHz tuning range and low phase noise," IEEE J. Solid-State Circuits, vol.36, no.1, pp.142–146, Jan. 2001.
[20] J. Maget, M. Tiebout, and R. Kraus, "Influence of novel MOS varactors on the performance of a fully integrated UMTS VCO in standard 0.25-μm CMOS technology," IEEE J. Solid-State Circuits, vol.37, no.7, pp.935–958, July 2002.
[21] N.H.W. Fong, J.-O. Plouchart, N. Zamder, D. Liu, L.F. Wagner, C. Plett, and N.G. Tarr, "Design of wide-band CMOS VCO for multiband wireless LAN applications," IEEE J. Solid-State Circuits, vol.38, no.8, pp.1333–1342, Aug. 2003.
[22] H.-R. Kim, C.-Y. Cha, S.-M. Oh, M.-S. Yang, and S.-G. Lee, "A very low-power quadrature VCO with back-gate coupling," IEEE J. Solid-State Circuits, vol.39, no.6, pp.952–955, June 2004.
[23] A.D. Berny, A.M. Niknejad, and R.G. Meyer, "A 1.8-GHz *LC* VCO with 1.3-GHz tuning range and digital amplitude calibration," IEEE J. Solid-State Circuits, vol.40, no.4, pp.909–917, April 2005.
[24] K. Kwok and H.C. Luong, "Ultra-low-voltage high-performance CMOS VCOs using transformer feedback," IEEE J. Solid-State Circuits, vol.40, no.3, pp.652–660, March 2005.
[25] P. Andreani, X. Wang, L. Vandi, and A. Fard, "A study of phase noise in Colpitts and *LC*-tank CMOS oscillators," IEEE J. Solid-State Circuits, vol.40, no.5, pp.1107–1118, May 2005.

Ching-Yuan Yang was born in Miaoli, Taiwan, R.O.C., in 1967. He received the B.S. degree in electrical engineering from the Tatung Institute of Technology, Taipei, Taiwan, R.O.C., in 1990, and the M.S. and Ph.D. degrees in electrical engineering from National Taiwan University, Taipei, in 1996 and 2000, respectively. During 2000–2002, he was on the faculty of Huafan University, Taipei, Taiwan. Since 2002, he has been on the faculty of National Chung Hsing University, Taichung, Taiwan, where he is currently an Assistant Professor with the Department of Electrical Engineering. His research interests are in the area of mixed-signal integrated circuits and systems for high-speed interfaces and wireless communication.

Meng-Ting Tsai received the B.S. degree in electrical engineering from National Chung Hsing University, Taichung, Taiwan, in 2004. He is currently working toward the M.S. degree in electrical engineering at National Chung Hsing University. His current research interests include analog and RF design, frequency synthesizers, and wireless communication.